Minimum Uncertainties in Position and Velocity Determination using x-ray Photons From Millisecond Pulsars

Neil Ashby, *Dept. of Physics, University of Colorado*
A. Robert Golshan, *Johns Hopkins University Applied Physics Laboratory*

BIOGRAPHY

Neil Ashby received a B.A. degree from the University of Colorado in 1955 and a Ph. D. from Harvard University in 1961. He served on the Faculty in the Dept. of Physics, University of Colorado at Boulder from 1962 to 2003 and currently is an Affiliate of the National Institute of Standards and Technology in Boulder, CO where he works on relativistic effects and noise in clocks, time scales, and navigation. He has contributed numerous studies of relativistic effects in the Global Positioning System. He has received several service awards from the University of Colorado including the University of Colorado Alumni Foundation Norlin Medal, May 2005. In January 2006 he received the F. K. Richtmyer Award of the American Association of Physics Teachers.

Robert Golshan was formerly a senior professional staff at the Space Department of the Johns Hopkins University Applied Physics Laboratory. Starting in February of 2008 he will be working at the Aerospace Corporation in El Segundo, CA. He has more than ten years of experience in analysis, simulation, and design of satellite communication systems. He received his B.S. and M.S. degrees from the University of Virginia and holds a Ph.D. from the University of Southern California all in Electrical Engineering.

ABSTRACT

Position determination of a spacecraft far from earth can be aided by binning the times of arrival of x-ray photons from a millisecond pulsar and matching the pulse shape to a standard shape by adjusting the phase of the observed signal. Usually studies of such measurements assume the frequency of the incoming signal is known, and show that the uncertainty in the component of position vector along the line of sight varies as $T_{obs}^{-1/2}$ where T_{obs} is the total observation time. Here we extend such analyses to include determination of velocity. Cramer-Rao lower bounds on the uncertainties of position and velocity are derived based on analysis of the Fisher Information Matrix. In one spatial dimension, the results can be expressed in terms of a minimal ellipse in position-velocity space whose size and orientation are determined by the observation time and by a single quantity depending on the standard pulse shape. For long observation times, the area of this ellipse decreases as T_{obs}^{-2}. If position were known, the uncertainty in velocity would decrease as $T_{obs}^{-3/2}$. If the spacecraft acceleration can be neglected, then by Liouville's theorem between measurements the area of the ellipse remains constant while its shape elongates in the position dimension. Another measurement of position and velocity may be combined with this minimum uncertainty ellipse to reduce the area further. Sequences of measurements can be used either as inputs to a Kalman filter, or described in terms of a set of recurrence relations for the parameters of the minimum uncertainty ellipse. We shall discuss the derivation of these results and some simulations based on this theory.

I. INTRODUCTION

Many studies of navigation based on binning the times-of-arrival (TOAs) of x-ray photons from pulsars concentrate on determining the phase of the incoming signal, (the phase determines the detector position) assuming the frequency of the signal pulses is known. On the other hand position and velocity go hand-in-hand in most orbit determination procedures. In this paper we study the determination of velocity as well as position and demonstrate that position cannot be accurately determined unless the detector velocity is either known or determined from the same data used to determine position. This paper is restricted to one spatial dimension; position and velocity can then be pictured in a two-dimensional "phase space" in which velocity is plotted vertically and position is plotted horizontally.

To illustrate the problem, Figure 1 gives five plots of binned TOA counts from the Crab pulsar signal, measured by the USA detector, after reduction of the measurements to the solar system barycenter. A total of

1,415,710 counts were received in 389.8 s, and the counts were accumulated into 1024 bins. The known frequency of the Crab signal was f_0 =29.8426722111886 Hz. The center plot in Figure 1 was binned using a period $1/f_0$. Background counts due to the Crab nebula have not been subtracted out. The two plots nearest to the central plot correspond to fractional frequency offsets of only one part in 10^5, due possibly to longitudinal Doppler shifts resulting from detector motion. One may observe from these two plots that the positions of the peaks—and hence the measured phase of the signal—is strongly correlated with the frequency error and hence with the velocity error, $\delta v/c$. We shall discuss this correlation in a later section. The sought-after peak is almost completely washed out when the fractional error in frequency reaches five parts in 10^5 in this example. Clearly accurate determination of signal phase is strongly dependent on knowledge of the signal frequency, and hence on knowledge of the detector velocity.

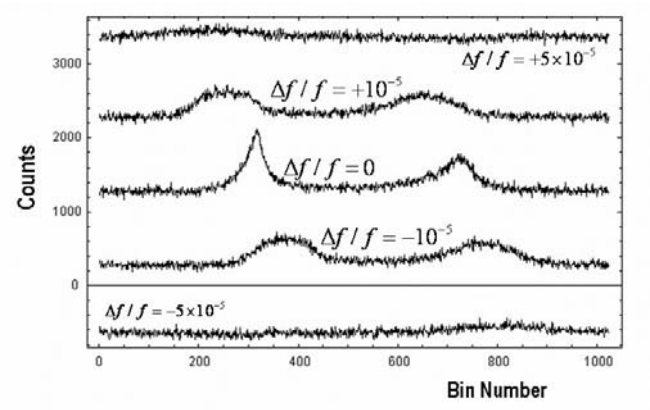

Figure 1. 1024-bin measurements of the Crab pulsar signal assuming different frequencies. The five plots, in order from bottom to top, assume fractional frequency offsets of $(-5,-1,0,+1,+5)\times10^{-5}$, respectively. No backgrounds have been subtracted out. Constant offsets of (-2000, -1000, 0, +1000, and +2000) have been added to the respective plots so that the plots are easier to see.

The outline of this paper is as follows: in Sect. II, we develop the theory of the Cramer-Rao lower bound on determination of both position and velocity, assuming Poisson statistics for the noise in the counts. For a measurement lasting a large number of periods, the minimum uncertainties in position and velocity, and the correlation between position and velocity, are simply related and a single integral suffices to characterize both uncertainties and their correlation. In Sect. III we show how, after a measurement update, the uncertainty in position will evolve in time due to the uncertainty in velocity effectively causing the ellipse to elongate in the spatial direction. In Sect. IV we discuss a possible sequence of measurements of both position and velocity, lasting for an observation time T_{obs}, followed by evolution of the uncertainties in position and velocity for a time ΔT, then another measurement, and so on. We shall describe the minimum uncertainties in terms of an ellipse in phase space. Sect. V discusses how a subsequent measurement can be combined with the time-dependent ellipse, and a set of recurrence relations are derived that can be used to describe a sequence of measurements in terms of evolving ellipses. Simulations are discussed in Sect. VI.

II. CRAMER-RAO LOWER BOUND

In the following, we shall limit the scope of our analysis to one spatial dimension by considering a detector traveling at a constant velocity along the pulsar's line of sight. Let x and v represent the position and velocity parameters to be determined from the photon TOA measurements taken over the interval (t_1, t_2) of duration $T_{obs} = t_2 - t_1$. Suppose that the source frequency f_0 is a known constant, and that the pulsar phase, denoted ϕ_0, is also known at some reference location, x_0, and time epoch, t_0. We shall take the reference point to be at the origin, $x = 0$, and the epoch at which the phase is ϕ_0 to be $t = 0$. The observed phase and frequency of the pulsar signal are then related to the position and velocity of the detector according to:

$$\phi = \phi_0 + f_0\left(t_1 + x/c\right) \tag{2.1}$$

$$f = f_0\left(1 + v/c\right) \tag{2.2}$$

where x is the detector position, and ϕ is the observed phase, both defined at the start of the observation, at time t_1; f is the observed frequency due to detector motion toward the source. The above relationships can be used to solve for position and velocity given estimates of the observed phase and frequency, and vice versa. We shall use the notation, $\phi(x)$ and $f(v)$, or more compactly, ϕ_x and f_v, to refer to these relationships. The TOA of x-ray photons may now be modeled as a Poisson point process with a periodic rate function of the form:

$$\lambda(t; x, v) \equiv (1 + v/c)\left[\alpha\, h\left(\phi_x + f_v\,(t - t_1)\right) + \beta\right], \quad t \in (t_1, t_2) \tag{2.3}$$

where α and β denote the arrival rates of the source and background photons at the reference point. The factor $(1 + v/c)$ arises because the count rates uniformly increase when the detector is in motion towards the source. The function $h(\phi)$ is the normalized dc-removed pulse profile of the source. It is usually defined on the phase interval, $\phi \in (0, 1\ \text{cycle})$, but its definition is

extended here to cover all phases by making it a periodic function, that is, by letting $h(m+\phi)=h(\phi)$ for all integers m. By definition, the function $h(\phi)$, satisfies the following two conditions:

$$\min_{\phi\in(0,1)} h(\phi)=0 \text{ , and } \int_0^1 h(\phi)\,d\phi=1 . \qquad (2.4)$$

We shall place the estimation parameters into a vector, $\boldsymbol{\theta}=\left[x,\, v\right]^{\mathrm{T}}$, and use $\hat{\theta}_1$ and $\hat{\theta}_2$ to refer to estimates of position and velocity. Also, we shall transform the photon TOA measurements into an observation vector by partitioning the entire observation interval into N bins of duration δt, and placing the number of photons counted in each bin into the vector, $\mathbf{z}=\left[z_1, z_2, \ldots, z_N\right]^{\mathrm{T}}$, as illustrated in Figure 2. This transformation can be carried out with δt set arbitrarily small and the resulting number of bins, N, arbitrarily large.

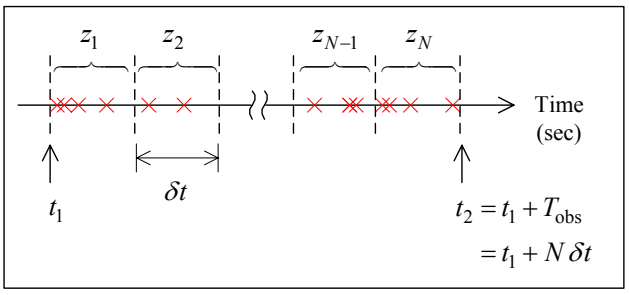

Figure 2. Photon binning and notation.

The Cramer-Rao lower bound for this problem is given by the formula [2,3]:

$$\mathrm{cov}\left(\hat{\boldsymbol{\theta}}\right) \geq \mathbf{I}^{-1}(\boldsymbol{\theta}) \qquad (2.5)$$

where $\hat{\boldsymbol{\theta}}$ is any unbiased vector estimate of $\boldsymbol{\theta}$ with $\mathrm{cov}(\hat{\boldsymbol{\theta}})$ denoting its covariance matrix, $\mathbf{I}(\boldsymbol{\theta})$ is the 2×2 Fisher information matrix, and the matrix inequality is understood in the sense that $\left(\mathrm{cov}\left(\hat{\boldsymbol{\theta}}\right) - \mathbf{I}^{-1}(\boldsymbol{\theta})\right)$ is positive semi-definite. The elements of the Fisher information matrix are given by:

$$\left[\mathbf{I}(\boldsymbol{\theta})\right]_{ij} = -\mathrm{E}\left(\frac{\partial^2 \ln p(\mathbf{z};\boldsymbol{\theta})}{\partial\theta_i\,\partial\theta_j}\right), \quad i,j=1,\,2 \qquad (2.6)$$

where the expectation is taken with respect to $p(\mathbf{z};\boldsymbol{\theta})$, using the true value of $\boldsymbol{\theta}$. For δt sufficiently small, the rate of arrival of photons over the n-th bin can be taken as constant:

$$\lambda_n(\boldsymbol{\theta}) \equiv \frac{1}{\delta t}\int_{t_1+(n-1)\,\delta t}^{t_1+n\,\delta t} \lambda\left(t;x,v\right)\,dt \qquad (2.7)$$

The bin count, z_n, is a Poisson random variable with probability mass function (pmf):

$$p\left(z_n=z;\,\boldsymbol{\theta}\right)=\frac{\left(\lambda_n(\boldsymbol{\theta})\;\delta t\right)^z}{z!}\exp\left(-\lambda_n(\boldsymbol{\theta})\;\delta t\right) , \quad z=0,\,1,\,2,\ldots \qquad (2.8)$$

For the Poisson distribution, the mean and variance are:

$$\mathrm{E}(z_n)=\mathrm{var}(z_n)=\lambda_n(\boldsymbol{\theta})\,\delta t . \qquad (2.9)$$

Since z_n is an independent random sequence, the joint pmf of the sequence is the product of the pmfs of the individual random variables in the sequence:

$$p(\mathbf{z};\boldsymbol{\theta})=\prod_{n=1}^{N}\frac{\left(\lambda_n(\boldsymbol{\theta})\,\delta t\right)^{z_n}}{z_n\,!}\exp\left(-\lambda_n(\boldsymbol{\theta})\,\delta t\right). \qquad (2.10)$$

We now proceed to evaluate the right-hand side of Eq. (2.6):

$$\ln p(\mathbf{z};\boldsymbol{\theta})=\sum_{n=1}^{N} z_n \ln\left(\lambda_n(\boldsymbol{\theta})\,\delta t\right)-\ln\left(z_n\,!\right)-\lambda_n(\boldsymbol{\theta})\,\delta t \qquad (2.11)$$

$$-\mathrm{E}\left(\frac{\partial^2 \ln p(\mathbf{z};\boldsymbol{\theta})}{\partial\theta_i\,\partial\theta_j}\right)=\sum_{n=1}^{N}\frac{\partial^2\lambda_n(\boldsymbol{\theta})\delta t}{\partial\theta_i\,\partial\theta_j}-\mathrm{E}(z_n)\frac{\partial^2\ln\left(\lambda_n(\boldsymbol{\theta})\delta t\right)}{\partial\theta_i\,\partial\theta_j} . \qquad (2.12)$$

Substituting Eq. (2.9) for $\mathrm{E}(z_n)$,

$$\mathrm{E}(z_n)\frac{\partial^2\ln\left(\lambda_n(\boldsymbol{\theta})\delta t\right)}{\partial\theta_i\,\partial\theta_j} = \lambda_n(\boldsymbol{\theta})\,\delta t\frac{\partial^2\ln\left(\lambda_n(\boldsymbol{\theta})\delta t\right)}{\partial\theta_i\,\partial\theta_j}$$

$$=\frac{\partial^2\lambda_n(\boldsymbol{\theta})\,\delta t}{\partial\theta_i\,\partial\theta_j}-\frac{1}{\lambda_n(\boldsymbol{\theta})\,\delta t}\left(\frac{\partial}{\partial\theta_i}\lambda_n(\boldsymbol{\theta})\,\delta t\right)\left(\frac{\partial}{\partial\theta_j}\lambda_n(\boldsymbol{\theta})\,\delta t\right) \qquad (2.13)$$

and Eq. (2.12) reduces to:

$$-\mathrm{E}\left(\frac{\partial^2 \ln p(\mathbf{z};\boldsymbol{\theta})}{\partial\theta_i\,\partial\theta_j}\right)=\sum_{n=1}^{N}\frac{1}{\lambda_n(\boldsymbol{\theta})}\,\frac{\partial\lambda_n(\boldsymbol{\theta})}{\partial\theta_i}\,\frac{\partial\lambda_n(\boldsymbol{\theta})}{\partial\theta_j}\,\delta t \qquad (2.14)$$

Since the bin size is arbitrarily small, we may now take the limit as $\delta t\to 0$ to obtain:

$$\left[\mathbf{I}(\boldsymbol{\theta})\right]_{ij}=\int_{t_1}^{t_2}\frac{\frac{\partial}{\partial\theta_i}\lambda(t;\boldsymbol{\theta})\;\frac{\partial}{\partial\theta_j}\lambda(t;\boldsymbol{\theta})}{\lambda(t;\boldsymbol{\theta})}\,dt , \quad i,j=1,\,2 \qquad (2.15)$$

The derivatives needed for evaluation of the components of $\mathbf{I}(\boldsymbol{\theta})$ are

$$\frac{\partial\lambda}{\partial x}=\frac{\partial\lambda}{\partial\theta_1}=(1+v/c)\frac{\alpha f_0}{c}h' ;$$
$$\frac{\partial\lambda}{\partial v}=\frac{\partial\lambda}{\partial\theta_2}=\frac{(\alpha h+\beta)}{c}+(1+v/c)\frac{\alpha f_0}{c}(t-t_1)h' . \qquad (2.16)$$

Evaluating I_{11}, after cancellations we obtain

$$I_{11} = (1+v/c)\frac{f_0^2}{c^2}\int_{t_1}^{t_2}\frac{(\alpha h')^2}{\alpha h+\beta}dt. \qquad (2.17)$$

The v/c correction is so small that it can be neglected here. We shall assume that the observation time T_{obs} is very large compared with the period $P = f_0^{-1}$ of the signal. The integrand of Eq. (2.17) is periodic so if we neglect contributions to the integral from fractions of a cycle near the endpoints, and the number of cycles of observation is N_c, then in each cycle we can let $t = nP + t'$ where n is an integer running from 1 to N_c. Then

$$I_{11} = \frac{f_0^2}{c^2}\sum_{n=1}^{N_c}\int_{(n-1)P}^{nP}\frac{(\alpha h')^2}{\alpha h+\beta}\,dt' \qquad (2.18)$$

Lastly, we change the variable on integration so that the integration is over the phase from 0 to 1. Let $t' = P\phi$; then

$$I_{11} = \frac{f_0^2 P}{c^2}N_c\int_0^1\frac{(\alpha h')^2}{\alpha h+\beta}\,d\phi\,. \qquad (2.19)$$

The product $NP = T_{obs}$, the observation time, so

$$I_{11} = \frac{f_0^2}{c^2}T_{obs}\int_0^1\frac{(\alpha h')^2}{\alpha h+\beta}\,d\phi\,. \qquad (2.20)$$

Evaluation of the off-diagonal component of the information matrix using Eqs. (2.16) gives

$$I_{12} = I_{21} = \frac{f_0}{c^2}\int_{t_1}^{t_2}\alpha h'\,dt + \frac{f_0^2}{c^2}(1+v/c)\int_{t_1}^{t_2}\frac{(\alpha h')^2}{\alpha h+\beta}(t-t_1)\,dt. \qquad (2.21)$$

Again we may neglect the v/c correction term and contributions to the integrals from fractions of a cycle near the endpoints. The first integral in Eq. (1.20) then vanishes because of the periodicity of h and its derivatives. Making use of the periodicity of the rate function, we can integrate over a single cycle if we let $t = nP + t' = (n+\phi)P$; then

$$\begin{aligned} I_{12} &= \frac{f_0}{c^2}\sum_{n=1}^{N_c}\int_0^P\frac{(\alpha h')^2}{\alpha h+\beta}(nP+t')\,dt' \\ &= \frac{f_0 P^2}{c^2}\sum_{n=1}^{N_c}\int_0^1\frac{(\alpha h')^2}{\alpha h+\beta}(n+\phi)\,d\phi \\ &= \frac{f_0 P^2}{2c^2}N_c(N_c+1)\int_0^1\frac{(\alpha h')^2}{\alpha h+\beta}d\phi + \frac{f_0 P^2}{2c^2}N_c\int_0^1\frac{(\alpha h')^2}{\alpha h+\beta}\phi\,d\phi. \end{aligned} \qquad (2.22)$$

Since $\phi < 1$, the second integral is smaller than the first. Also, we are assuming $N_c >> 1$, so the first term dominates and to a very good approximation we obtain

$$I_{12} = \frac{1}{2}\frac{f_0}{c^2}T_{obs}^2\int_0^1\frac{(\alpha h')^2}{\alpha h+\beta}d\phi. \qquad (2.23)$$

The integral that appears in this expression is the same one that determines I_{11}. This trend continues with the evaluation of I_{22} when similar approximations are made.

After substituting from the second of Eqs. (2.16), squaring, neglecting v/c corrections and small contributions from fractions of a cycle near the endpoints, and letting $t = (n+\phi)P$ we obtain

$$\begin{aligned} I_{22} = {} & \frac{P}{c^2}\sum_{n=1}^{N_c}\int_0^1(\alpha h+\beta)\,d\phi + \frac{2P^2}{c^2}\sum_{n=1}^{N_c}n\int_0^1\alpha h'\,d\phi \\ & + \frac{2f_0P^2}{c^2}\sum_{n=1}^{N_c}\int_0^1\alpha h'\phi\,d\phi + \frac{f_0^2P^3}{c^2}\sum_{n=1}^{N_c}n^2\int_0^1\frac{(\alpha h')^2}{\alpha h+\beta}d\phi \\ & + \frac{2f_0^2P^3}{c^2}\sum_{n=1}^{N_c}n\int_0^1\frac{(\alpha h')^2}{\alpha h+\beta}\phi\,d\phi + \frac{f_0^2P^3}{c^2}\sum_{n=1}^{N_c}\int_0^1\frac{(\alpha h')^2\phi^2}{\alpha h+\beta}d\phi. \end{aligned} \qquad (2.24)$$

When $N_c >> 1$, by far the largest contribution comes from the fourth term in Eq. (2.24). The result is

$$\begin{aligned} I_{22} = {} & \frac{f_0^2P^3}{c^2}\frac{N_c(N_c+1)(2N_c+1)}{6}\int_0^1\frac{(\alpha h')^2}{\alpha h+\beta}d\phi \\ & \approx \frac{1}{3}\frac{f_0^2}{c^2}T_{obs}^3\int_0^1\frac{(\alpha h')^2}{\alpha h+\beta}d\phi. \end{aligned} \qquad (2.25)$$

Thus, the same integral, characteristic of the signal, determines all the elements of the Fisher information matrix. If we define

$$L \equiv \int_0^1\frac{(\alpha h')^2}{\alpha h+\beta}d\phi\,, \qquad (2.26)$$

then the inverse of the fisher information matrix is

$$\mathbf{I}^{-1}(\boldsymbol{\theta}) = \frac{c^2}{f_0^2 L}\begin{pmatrix} 4/T_{obs} & -6/T_{obs}^2 \\ -6/T_{obs}^2 & 12/T_{obs}^3 \end{pmatrix}. \qquad (2.27)$$

III. IDENTIFICATION AND EVOLUTION OF PHASE SPACE UNCERTAINTY ELLIPSE

To aid in visualizing the implications of Eq. (2.27), we shall assume that the noise components giving rise to the minimum uncertainties are jointly Gaussian, and shall construct a probability density that has the same second moments as given by the covariances of Eq. (2.5). The

probability density will be of the form of a bivariate normal distribution, and apart from normalization is

$$\exp\left(-\frac{1}{1-\rho^2}\left(\frac{x^2}{2\sigma_x{}^2}-\frac{\rho xv}{\sigma_x\sigma_v}+\frac{v^2}{2\sigma_v{}^2}\right)\right), \qquad (3.1)$$

where we have assumed the mean values of x and v are zero; this assumption is only to simplify the calculations and is not essential. The normalization constant for the distribution, Eq. (3.1) is $(2\pi\sigma_x\sigma_y\sqrt{1-\rho^2})^{-1}$. The probability density will fall to $1/e$ of its maximum value on the ellipse described by the equation

$$\frac{1}{1-\rho^2}\left(\frac{x^2}{2\sigma_x{}^2}-\frac{\rho xv}{\sigma_x\sigma_v}+\frac{v^2}{2\sigma_v{}^2}\right)=1. \qquad (3.2)$$

We shall use this ellipse as a model of the region in phase space within which the probability mass of the best unbiased estimator is concentrated—that is the meaning of the Cramer-Rao lower bound on the covariance matrix. The covariance matrix corresponding to this distribution is

$$\Sigma=\begin{pmatrix}\sigma_x^2 & \rho\sigma_x\sigma_v\\ \rho\sigma_x\sigma_v & \sigma_v^2\end{pmatrix}. \qquad (3.3)$$

We identify these constants with the minimum expectation values given by the inverse of the Fisher information matrix. We then find after some calculation that

$$\begin{aligned}\sigma_x^2 &= 4\left(\frac{c}{f_0}\right)^2\frac{1}{T_{obs}L};\\ \sigma_v^2 &= 12\left(\frac{c}{f_0}\right)^2\frac{1}{T_{obs}^3L};\\ \rho\sigma_x\sigma_v &= -6\left(\frac{c}{f_0}\right)^2\frac{1}{T_{obs}^2L},\end{aligned} \qquad (3.4)$$

which give

$$\rho=-\sqrt{\frac{3}{4}}. \qquad (3.5)$$

Thus with the approximations made here, the coefficient of correlation between position and velocity for one measurement is a constant.

The velocity measurement is basically a measurement of the observed signal frequency, and the uncertainty in this measurement decreases as $T_{obs}^{-3/2}$. Such dependence on observation time is typically associated with measurement noise [4]—in the present case, it is due to counting statistics.

IV. ELLIPSE EVOLUTION BETWEEN UPDATES

Now we follow the ellipse through its evolution between measurement updates. According to Liouville's theorem, the area of a region in phase space, when no acceleration acts, will be conserved. An ellipse described by the parameters of Eq. (3.2) has area

$$A=2\pi\sqrt{1-\rho^2}\,\sigma_x\sigma_v. \qquad (4.1)$$

In the absence of additional information, with no acceleration a point (x,v) on the ellipse will move during a time ΔT to $(x+v\Delta T,v)$. The ellipse will elongate in the direction of the $x-$axis and will be described by a new equation:

$$\frac{1}{1-\rho^2}\left(\frac{(x-v\Delta T)^2}{2\sigma_x{}^2}-\frac{\rho(x-v\Delta T)v}{\sigma_x\sigma_v}+\frac{v^2}{2\sigma_v{}^2}\right)=1. \qquad (4.2)$$

This is equivalent to an ellipse with new parameters:

$$\left[\frac{1}{1-\rho^2}\left(\frac{x^2}{2\sigma_x{}^2}-\frac{\rho xv}{\sigma_x\sigma_v}+\frac{v^2}{2\sigma_v{}^2}\right)\right]_k^{(-)}=1. \qquad (4.3)$$

where we have introduced a new notation in order to make the equations more compact. Here the superscript "(-)" means that all constants inside the brackets are associated with the end of the evolution cycle, just before the k^{th} measurement update. Similarly the ellipse parameters after a measurement update will be denoted with a superscript "(+)". We regard an event step, labeled by k, in the measurement process, as consisting of the result of evolution until just before an update, followed by an update. An uncertainty such as σ_x during this process would be denoted at the end of the evolution by $[\sigma_x]_k^{(-)}$ and after update k by $[\sigma_x]_k^{(+)}$, and after the next update by $[\sigma_x]_{k+1}^{(+)}$. With these conventions, the parameters of the evolving ellipse are obtained by identifying Eqs. (4.3) and (4.2), and are

$$\begin{aligned}[\sigma_v]_k^{(-)} &= [\sigma_v]_{k-1}^{(+)};\\ [\sigma_x]_k^{(-)} &= \left[\sqrt{\sigma_x^2+2\rho\sigma_x\sigma_v\Delta T+\sigma_v^2\Delta T^2}\right]_{k-1}^{(+)};\\ [\rho]_k^{(-)} &= \left[\frac{\rho\sigma_x+\sigma_v\Delta T}{\sqrt{\sigma_x^2+2\rho\sigma_x\sigma_v\Delta T+\sigma_v^2\Delta T^2}}\right]_{k-1}^{(+)}.\end{aligned} \qquad (4.4)$$

If ΔT varies from step to step, then the notation allows the index $k-1$ also to be attached to ΔT during evolution.

The minimum uncertainty in the velocity direction does not change during the evolution, as one would expect. The area of the evolving ellipse, from Eq. (4.1), is

$$A = \left[2\pi\sqrt{1-\rho^2}\,\sigma_x\sigma_v \right]_k^{(-)} = \left[2\pi\sqrt{1-\rho^2}\,\sigma_x\sigma_v \right]_{k-1}^{(+)}, \quad (4.5)$$

after using the solutions (4.4).

V. RECURRENCE RELATIONS

We next investigate the modification of the minimum uncertainty ellipse when another measurement is made and the uncertainty information is updated. This will be done for a general k. Assume that at some point after k steps in the sequence of measurement, evolution, measurement, evolution, etc., and just before a measurement update the minimum uncertainty ellipse is described by Eq. (4.3).

Then suppose that another measurement of position and velocity is obtained by binning the TOAs of photons from the source. By itself, this measurement would be described by a probability density similar to Eq. (3.1). The result of the evolution is also represented by a probability density of this form. We assume these probability densities are independent and combine them by multiplying densities; this is equivalent to adding exponents. Addition of two quadratic forms in (x, v) gives another quadratic form, and we can identify the resulting form as determining another ellipse corresponding to the end of step k in the sequence. Identifying the parameters of the resulting ellipse by labels k and (+) gives the following set of equations:

$$\begin{aligned}
\left[\frac{1}{1-\rho^2}\frac{1}{\sigma_x^2} \right]_k^{(+)} &= \left[\frac{1}{1-\rho^2}\frac{1}{\sigma_x^2} \right]_k^{e} + \left[\frac{1}{1-\rho^2}\frac{1}{\sigma_x^2} \right]_k^{(-)}; \\
\left[\frac{1}{1-\rho^2}\frac{\rho}{\sigma_x\sigma_v} \right]_k^{(+)} &= \left[\frac{1}{1-\rho^2}\frac{\rho}{\sigma_x\sigma_v} \right]_k^{e} \\
&\quad + \left[\frac{1}{1-\rho^2}\left(\frac{\rho}{\sigma_x\sigma_v} + \frac{\Delta T}{\sigma_x^2} \right) \right]_k^{(-)}; \\
\left[\frac{1}{1-\rho^2}\frac{1}{\sigma_v^2} \right]_k^{(+)} &= \left[\frac{1}{1-\rho^2}\frac{1}{\sigma_v^2} \right]_k^{e} \\
&\quad + \left[\frac{1}{1-\rho^2}\left(\frac{1}{\sigma_v^2} + \frac{2\rho\Delta T}{\sigma_x\sigma_v} + \frac{\Delta T^2}{\sigma_x^2} \right) \right]_k^{(-)}.
\end{aligned} \quad (5.1)$$

On the right, the superscript "e" means the independent experimentally determined values of the ellipse parameters obtained by binning TOAs at step k. Then the updated ellipse parameters just after the k update are on the left sides. These equations can be solved explicitly for the ellipse parameters at the beginning of step $k+1$. The algebra is lengthy and will not be given here. The results are expressed more easily if the following auxiliary quantities are defined:

$$\begin{aligned}
D_{x,k} &= \left[(1-\rho^2)\sigma_x^2 \right]_k^{e} + \left[(1-\rho^2)\sigma_x^2 \right]_k^{(-)}; \\
G_k^{(-)} &= \left[1 + \frac{2\rho\Delta T\sigma_v}{\sigma_x} + \left(\frac{\Delta T\sigma_v}{\sigma_x} \right)^2 \right]_k^{(-)} \\
D_{v,k} &= \left[(1-\rho^2)\sigma_v^2 \right]_k^{e} G_k^{(-)} + \left[(1-\rho^2)\sigma_v^2 \right]_k^{(-)};
\end{aligned} \quad (5.2)$$

Then we find

$$\begin{aligned}
[\rho]_k^{(+)} &= \frac{1}{\sqrt{D_{x,k+1}D_{v,k+1}}} \left(\begin{array}{c} \left[\rho + \dfrac{\Delta T\sigma_v}{\sigma_x} \right]_k^{(-)} \left[(1-\rho^2)\sigma_x\sigma_v \right]_k^{e} \\ + [\rho]_k^{e} \left[(1-\rho^2)\sigma_x\sigma_v \right]_k^{(-)} \end{array} \right); \\
\left[\sigma_x^2 \right]_k^{(+)} &= \left[\frac{1}{1-\rho^2} \right]_k^{(+)} \frac{\left[\left(1-\rho^2\right)\sigma_x^2 \right]_k^{e} \left[\left(1-\rho^2\right)\sigma_x^2 \right]_k^{(-)}}{D_{x,k}}; \\
\left[\sigma_v^2 \right]_k^{(+)} &= \left[\frac{1}{1-\rho^2} \right]_k^{(+)} \frac{\left[\left(1-\rho^2\right)\sigma_v^2 \right]_k^{e} \left[\left(1-\rho^2\right)\sigma_v^2 \right]_k^{(-)}}{D_{v,k}}.
\end{aligned} \quad (5.3)$$

The systems of equations (4.4), (5.3), provide a complete set of recurrence relations for a sequence of measurements. In the next section we apply these equations to an example of navigation along the line-of-sight to the Crab pulsar.

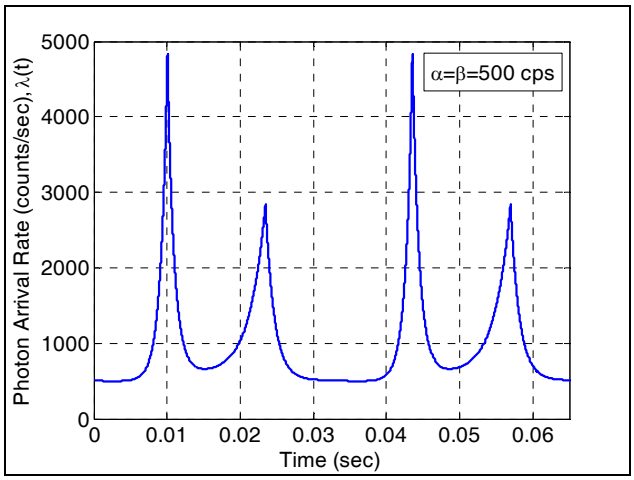

Figure 3. Intensity profile function used to model the Crab pulsar. The period is 33.5 ms. The time-averaged arrival rate of photons is $\alpha + \beta = 1000$ counts/sec.

VI. EXAMPLE—NAVIGATION USING CRAB PULSAR

In this example we use a model analytic expression for the pulse shape of the Crab pulsar, illustrated in Figure 3. For simplicity in this example we shall assume the time intervals between updates are all equal, $\Delta T = 360$ s. The time of observation, T_{obs}, is also assumed to be 360 s so that while measurements are being accumulated for this time interval, the ellipse parameters are evolving according to Eqs. (4.4). Each measurement gives the same information, determined by a single integral, Eq. (2.26). We use the profile in Figure 3 but assume there are 500 source counts/s and 500 background counts/s. These numbers are chosen for illustrative purposes only; in an actual situation the count rates will depend on that properties of the particular detector. In the present case the value of the integral L is

$$L = 2.873 \times 10^5 \, s^{-1}. \tag{6.1}$$

For the assumed observation time, the experimentally determined ellipse parameters after one measurement are obtained using the relationships in Eqs. (3.4) and (3.5),

$$\begin{aligned} [\sigma_x]_e &= 1975.65 \, \text{m}, \\ [\sigma_v]_e &= 9.505 \, \text{m/s}, \\ [\rho]_e &= -0.866 \end{aligned} \tag{6.2}$$

Thus after 360 s of observations the uncertainties in position and velocity are 1.98 km and 9.51 m/s, respectively and the correlation between them is $\rho = -0.866$.

The values of the ellipse parameters given in Eq. (6.2) are based on the Cramer-Rao lower bound evaluated using the Crab pulse profile. These theoretical predictions are now validated via a Monte Carlo simulation using the setup diagrammed in Figure 4. The true values of position and velocity are set to 3,350.90636 km and 10.0 km/s in the simulation. Photon TOAs are then generated as realizations of a non-homogeneous Poisson process with $\lambda(t; x, v)$ as the rate function. Estimates of the position and velocity parameters are obtained by processing the photon TOAs through the maximum likelihood estimator (MLE) described in reference [1].

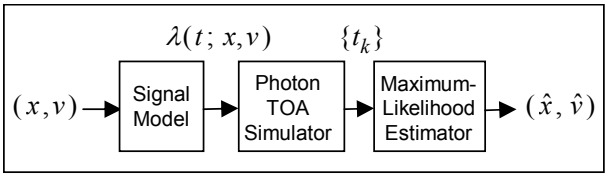

Figure 4. Simulation of photon TOAs using the Crab pulse profile and subsequent maximum likelihood estimation of position and velocity.

Figure 5 shows the result of the MLE simulation. A scatter plot of position vs. velocity estimation error is shown for 10,000 realizations of the photon TOAs over a 360 s observation interval. Figure 6 compares the ellipse parameters obtained via the MLE Monte-Carlo simulation against the Cramer-Rao theoretical predications.

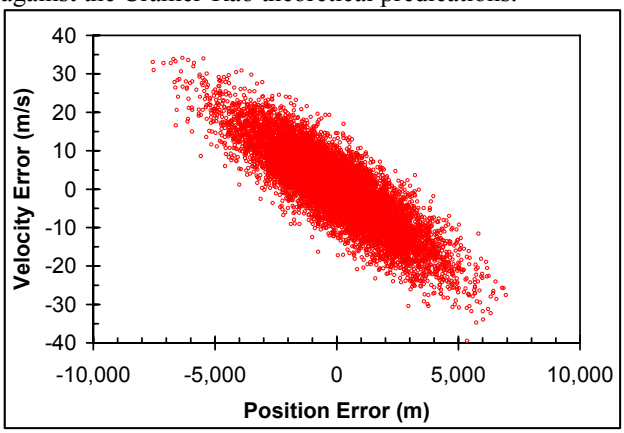

Figure 5. Scatter plot of the position vs. velocity estimation errors for 10,000 independent realizations of the photon TOAs over a 360 s observation interval processed through the MLE.

	Position RMS Error, $[\sigma_x]_e$ (m)	Velocity RMS Error, $[\sigma_v]_e$ (m/s)	Correlation Coefficient, $[\rho]_e$
MLE Simulation	2,046.25	9.935	-0.855
Cramer-Rao Theory	1,975.65	9.505	-0.866

Figure 6. Comparison of the MLE Monte-Carlo simulation vs. the Cramer-Rao theoretical results.

Figure 7 shows the uncertainty ellipse after the first measurement and its evolution after an additional 360 s. The correlation between position and velocity is reflected in the tilting of the axes. A positive error in v would correspond to a negative error in position, consistent with the binning results shown in Figure 1.

Figure 8 shows the minimum uncertainty ellipse evolved after 360 s and the result of a measurement update at that time. Figure 9 is a log-log plot of velocity uncertainties. The lower line is a plot of the velocity uncertainty given in Eq. (3.4) as a function of time showing the $T_{obs}^{-3/2}$ dependence on observation time. The upper line shows the results of measurement updates every 360 s, assuming that each measurement is independent and that phase information is lost after each measurement. This shows that in order to take advantage of the rapid decrease of velocity uncertainty, one must maintain the phase from

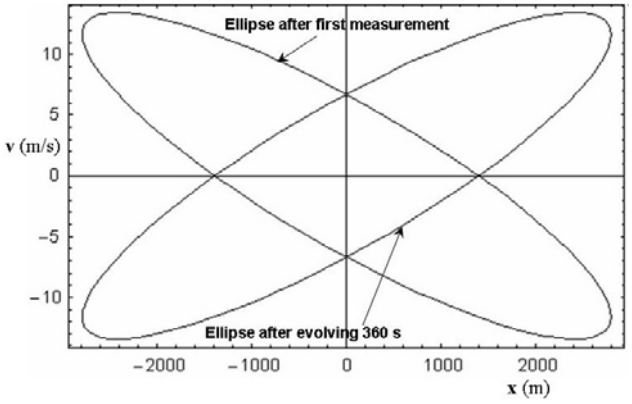

Figure 7. Uncertainty ellipse after one measurement lasting 360 s, and ellipse after subsequent evolution through 360 s.

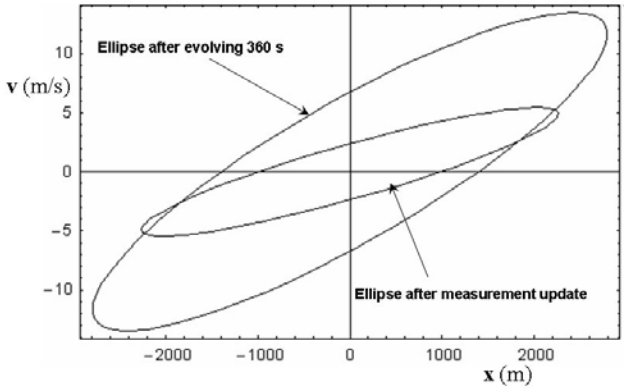

Figure 8. Minimum uncertainty ellipses after evolving for 360 s and then updating with a second set of observations.

one measurement interval to the next. During the total observation time of about a million seconds in this figure, there were 10000 measurement updates. The position uncertainty shown in Figure 10 decreases as the inverse square root of the total time, so the slope of the graph is -1/2 except during coasting intervals.

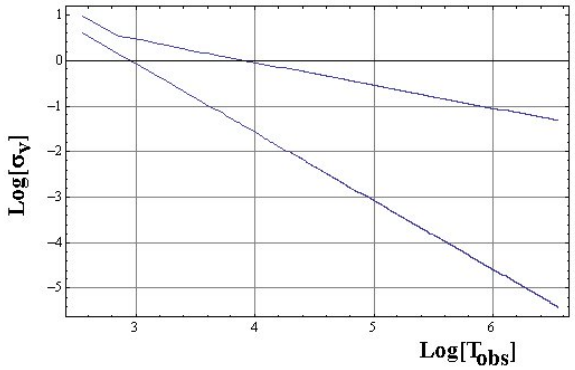

Figure 9. The lower straight line is a plot of Eq. (3.4), while the upper line shows the $T_{obs}^{-1/2}$ dependence that would result if independent measurements of 360 s duration are used with the recurrence relations. In the latter case phase information is lost at each update.

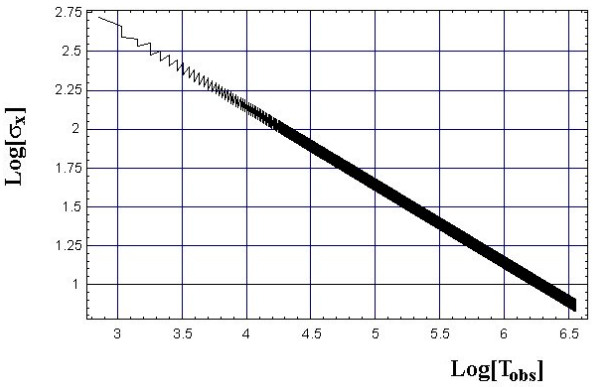

Figure 10. Plot of uncertainty in position using a series consisting of repeated measurements and updates, with no phase information carried forward from one time interval to the next.

VII. OTHER LINEAR COMBINATIONS

A quadratic form such as that in (3.1) can be diagonalized by choosing different linear combinations of parameters. In the present case, (3.1) is equivalent to

$$\exp\left[-\frac{1}{1-\rho^2}\left(\frac{1+\rho}{2}\frac{\left(x+\sigma_x v/\sigma_v\right)^2}{(2\sigma_x)^2}+\frac{1-\rho}{2}\frac{\left(x-\sigma_x v/\sigma_v\right)^2}{(2\sigma_x)^2}\right)\right] \tag{6.3}$$

as can readily seen by expanding the squares. One of the linear combinations,

$$x \pm \sigma_x v / \sigma_v, \tag{6.4}$$

has smaller uncertainty than the other. In the case of a single measurement lasting time T_{obs}, these linear combinations, from Eq. (3.4), are

$$x \pm \sigma_x v / \sigma_v = x \pm \frac{1}{\sqrt{3}} T_{obs} v. \tag{6.5}$$

The corresponding uncertainties are

$$\frac{\sigma_x}{\sqrt{1 \pm \rho}}. \tag{6.6}$$

These uncertainties correspond to the semi-major and semi-minor axes of the minimum uncertainty ellipse reduced to length units. However, we shall not make use of such linear combinations in this paper.

VIII. DISCUSSION

If the only parameter determined by the TOA observations were the phase, and hence the detector position, the resulting uncertainty would be smaller by a factor of 2. This factor is a penalty imposed by the theory, when two parameters are to be determined.

REFERENCES

1. A. R. Golshan and S. I. Shiekh, "On pulse phase estimation and tracking of variable celestial X-ray sources," Proc. ION 63rd Annual Meeting, April 23-25, 2007, Cambridge, MA, pp 413-422.
2. S. M. Kay, Fundamentals of Statistical Signal Processing: Estimation Theory, Chapter 3, Prentice-Hall, New Jersey, (1993).
3. H. Cramer, Mathematical Methods of Statistics, Princeton University Press, pp 490-495 (1954).
4. V. M. Kaspi, J. H. Taylor and M. F. Ryba, Astro-physical Journal, 428, 713, (1994).